DROUGHT

A global transition to flash droughts under climate change

Xing Yuan[1,2]*, Yumiao Wang[1,2], Peng Ji[1,2], Peili Wu[3], Justin Sheffield[4], Jason A. Otkin[5]

Flash droughts have occurred frequently worldwide, with a rapid onset that challenges drought monitoring and forecasting capabilities. However, there is no consensus on whether flash droughts have become the new normal because slow droughts may also increase. In this study, we show that drought intensification rates have sped up over subseasonal time scales and that there has been a transition toward more flash droughts over 74% of the global regions identified by the Intergovernmental Panel on Climate Change Special Report on Extreme Events during the past 64 years. The transition is associated with amplified anomalies of evapotranspiration and precipitation deficit caused by anthropogenic climate change. In the future, the transition is projected to expand to most land areas, with larger increases under higher-emission scenarios. These findings underscore the urgency for adapting to faster-onset droughts in a warmer future.

Droughts are periods of time with a persistent water deficit (*1*, *2*), which can cause devastating impacts on regional economies and environments (*3*–*5*), as well as on human health (*6*). Droughts mainly originate from large-scale internal climate variability, in which ocean-atmosphere teleconnections associated with phenomena such as the El Niño–Southern Oscillation, Pacific Decadal Variability, and Atlantic Multidecadal Variability play critical roles in drought formation and persistence over interannual to decadal time scales (*7*, *8*). For droughts that occur over shorter seasonal time scales, the dominant drivers can also include local or remote land-atmosphere feedbacks (*9*, *10*). The multiscale interactions among these different parts of the climate system raise challenges for drought forecasting and impact mitigation. Droughts are also influenced by anthropogenic forcings such as climate change (*2*, *11*), land use or land cover change, and human water consumption and management (*12*, *13*). As global warming accelerates the terrestrial water cycle (*14*, *15*), agricultural and hydrological droughts have increased substantially in many regions (*11*, *16*, *17*) and are projected to become more frequent, longer, and more severe in a warmer future (*2*, *11*, *18*). Such statements are based on analysis of droughts at seasonal, annual, or decadal time scales. However, recent studies have shown that droughts also occur frequently at subseasonal time scales worldwide (*4*, *5*, *19*–*24*) and can develop into severe droughts within a few weeks. These rapid-onset droughts are termed "flash droughts" in contrast with conventional droughts that evolve slowly. In addition to large precipitation deficits, flash droughts are also caused by abnormally high evapotranspiration that depletes soil water quickly (*25*–*29*), which challenges current drought monitoring and forecasting capabilities (*30*–*34*) that were developed to detect slowly evolving droughts.

The concept of flash droughts was proposed at the beginning of the 21st century but did not receive wide attention until the occurrence of the severe US drought in the summer of 2012 (*5*, *28*, *30*, *34*). This drought was regarded as one of the most severe US droughts since the 1930s Dust Bowl and caused more than US$30 billion of economic losses (*35*). One of the distinctive features of this drought was its extremely rapid onset, with many locations going from drought-free to extreme drought conditions within a month. This rapid intensification was unexpected, and no operational prediction models captured its onset (*30*). In this regard, some flash droughts can be considered as the onset stage of a long-term drought, the impacts of which are amplified by a subsequent persistent period of severe drought conditions (*23*, *30*, *36*). Moreover, even without a transition to seasonal drought, these rapidly evolving subseasonal droughts have substantial impacts on vegetation growth (*37*) and can trigger compound extreme events such as heat waves or wildfires. Previous studies have focused on the evolution and changing characteristics of flash droughts (*5*, *20*–*29*) and found that human-induced climate change has increased the frequency of flash droughts throughout southern Africa (*20*) and China (*21*). A recent study presents a 36-year climatology report of global flash droughts and shows substantial increases in flash droughts throughout several key regions (*38*). However, no consensus has been reached on whether there has been a transition from slow to flash droughts at the global scale, because the frequency of slower-developing droughts at subseasonal time scales may also increase. There is currently no robust evidence that drought intensification rates have increased globally, although several studies have speculated such increases by relating drought onset with global warming (*16*, *21*).

In this study, we investigated changes in the speed of global drought onset and the partitioning between flash and slow droughts. We divided subseasonal droughts into flash droughts (*21*, *28*) and slow droughts by onset speed measured by the declining rate of soil moisture and present their global distributions during the local growing season over the past 64 years. We then estimated the global trend of the ratio of the number of flash droughts to total subseasonal droughts and the global trend of the onset speed of subseasonal droughts and attributed these trends to anthropogenic climate change on the basis of the sixth Coupled Model Intercomparison Project (CMIP6) (*39*) climate model simulations (table S1). We also showed how these trends vary over different IPCC SREX (Intergovernmental Panel on Climate Change Special Report on EXtreme events) regions (*40*).

Global distributions of flash and slow droughts

On the basis of estimates of soil moisture from three global reanalyses from 1951 to 2014, subseasonal drought events are identified as pentad-mean soil moisture declines from above the 40th percentile to below the 20th percentile and then increase to above the 20th percentile again [supplementary materials (SM), materials and methods]. The minimum duration for subseasonal droughts is 20 days to exclude dry spells that are too short to cause substantial impacts. We then divided the subseasonal droughts into flash and slow droughts depending on the rate of the reduction in soil moisture (*21*) during the onset stage (fig. S1). We used the ratio of flash drought events to the total number of subseasonal drought events, and the subseasonal drought onset speed (SM, materials and methods), to quantify the transition to flash droughts by determining whether there are significant trends in these two indices. Flash droughts tend to occur more often than slow droughts over humid regions with lower aridity (Fig. 1A and fig. S2), where flash-drought frequency is two to three times greater than other regions (fig. S3A). By contrast, slow drought occurrence has smaller spatial variability (fig. S3B). Flash droughts usually last for 30 to 45 days, whereas slow droughts usually last for 40 to 60 days (fig. S4). The uncertainty across

[1]School of Hydrology and Water Resources, Nanjing University of Information Science and Technology, Nanjing 210044, Jiangsu, China. [2]Key Laboratory of Hydrometeorological Disaster Mechanism and Warning of Ministry of Water Resources/Collaborative Innovation Center on Forecast and Evaluation of Meteorological Disasters, Nanjing University of Information Science and Technology, Nanjing 210044, Jiangsu, China. [3]Met Office Hadley Centre, Exeter EX1 3PB, UK. [4]Geography and Environmental Science, University of Southampton, Southampton SO17 1BJ, UK. [5]Cooperative Institute for Meteorological Satellite Studies, Space Science and Engineering Center, University of Wisconsin–Madison, Madison, WI 53706, USA.
*Corresponding author. Email: xyuan@nuist.edu.cn

the three reanalyses is low over most humid and semihumid regions but high over arid regions (fig. S5).

The regions with a higher flash drought ratio also have faster drought onset speeds (Fig. 1B), which are associated with large precipitation deficits and/or increases in evapotranspiration. Compared with slow droughts, larger precipitation deficits occur during the onset stage of flash droughts over most global land areas (fig. S6A). In addition to the precipitation deficit, the increase in evapotranspiration (fig. S6B) accelerates the drawdown of soil moisture, which results in a higher likelihood of flash drought over humid regions, such as Europe, North Asia, southern China, eastern and northwestern parts of North America, and the Amazon. Evapotranspiration over these regions is energy limited, and the enhanced radiation because of fewer clouds drives the increase in evapotranspiration and speeds up drought onset. Over regions with higher aridity (such as northern China, western India, and parts of Africa), evapotranspiration is water limited (*41*), and the decrease in evapotranspiration during the onset stage suggests that precipitation deficit is the main driver of flash droughts (fig. S6).

Detection and attribution of changes in global droughts

Given that global land evapotranspiration is increasing in a warming climate (*14*, *42*), it was hypothesized that drought onset may speed up globally (*16*). In this study, we provide robust estimations that there are upward trends in the global mean flash drought ratio ($P < 0.1$) and subseasonal drought onset speed ($P < 0.1$) from 1951 to 2014 (Fig. 2, A and B), which means that subseasonal droughts have developed faster and shifted from slow to flash droughts at global scale. To assess whether the global trends are sensitive to the definition of flash droughts (*43*), we increased and decreased the soil moisture thresholds for drought starting and ending points as well as drought onset speed and found that the upward global trends remain significant ($P < 0.1$) (fig. S7).

The upward global trends are well captured by the state-of-the-art CMIP6/ALL multi-model ensemble simulations ($P < 0.1$) (Fig. 2, A and B), in which both the anthropogenic climate forcings (anthropogenic emission of, for example, greenhouse gases and aerosols) and natural climate forcings (solar and volcanic activities) are considered. The CMIP6/ALL ensemble simulations also roughly capture the spatial patterns of long-term climatology of flash drought ratio and subseasonal drought onset speed (fig. S8). However, the global trends are not captured by the CMIP6/NAT ensemble simulations that only consider natural climate forcings (Fig. 2, A and B). The best estimates of scaling factors (SM, materials and methods) show that only the ANT (ALL-NAT; anthropogenic forcings) signal is detectable, with contributions of 48% (10 to 86%) and 39% (13 to 70%) to the increases in flash drought ratio and subseasonal drought onset speed, respectively (Fig. 2, C and D). With CMIP5 models included, the detection and attribution results remain similar (fig. S9). We therefore conclude that the global transition to more frequent flash droughts during the past 64 years is influenced by anthropogenic climate change.

During the onset stage of subseasonal droughts, there has been a significant increase ($P < 0.1$) in strong anomalies of global evapotranspiration and a significant decrease ($P < 0.1$) in strong anomalies of precipitation surplus (precipitation minus evapotranspiration) during the past 64 years, in which anthropogenic contributions are detectable (fig. S10). The decrease in strong anomalies of precipitation surplus is dominated by the increase in strong anomalies of evapotranspiration because strong anomalies of precipitation show a small and insignificant decreasing trend ($P < 0.1$). Again, the results were similar after incorporating CMIP5 models (fig. S11). Therefore, anthropogenic climate change has significantly ($P < 0.1$) amplified the strong anomalies of global evapotranspiration and precipitation surplus and ultimately

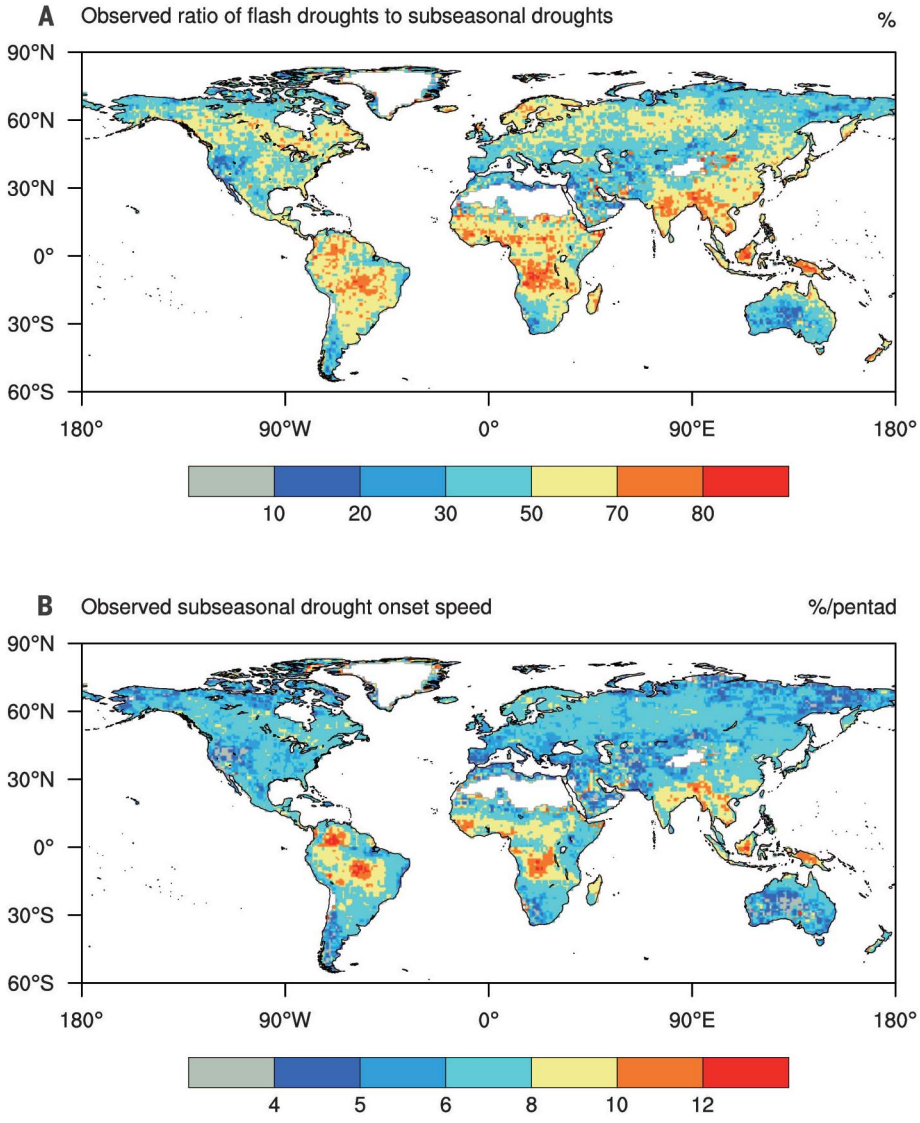

Fig. 1. Spatial distributions of the flash drought ratio and the onset speed of subseasonal droughts. (**A**) The ratio (%) of flash drought events to the sum of flash and slow drought events [subseasonal drought events (SM, materials and methods)]. (**B**) The mean onset speed (%/pentad) for both flash and slow droughts. All statistics are based on the average results from ERA5, GLDASv2.0/Noah, and GLDASv2.0/Catchment global reanalysis data during the growing seasons of 1951 to 2014 (April to September for the Northern Hemisphere and October to March for the Southern Hemisphere).

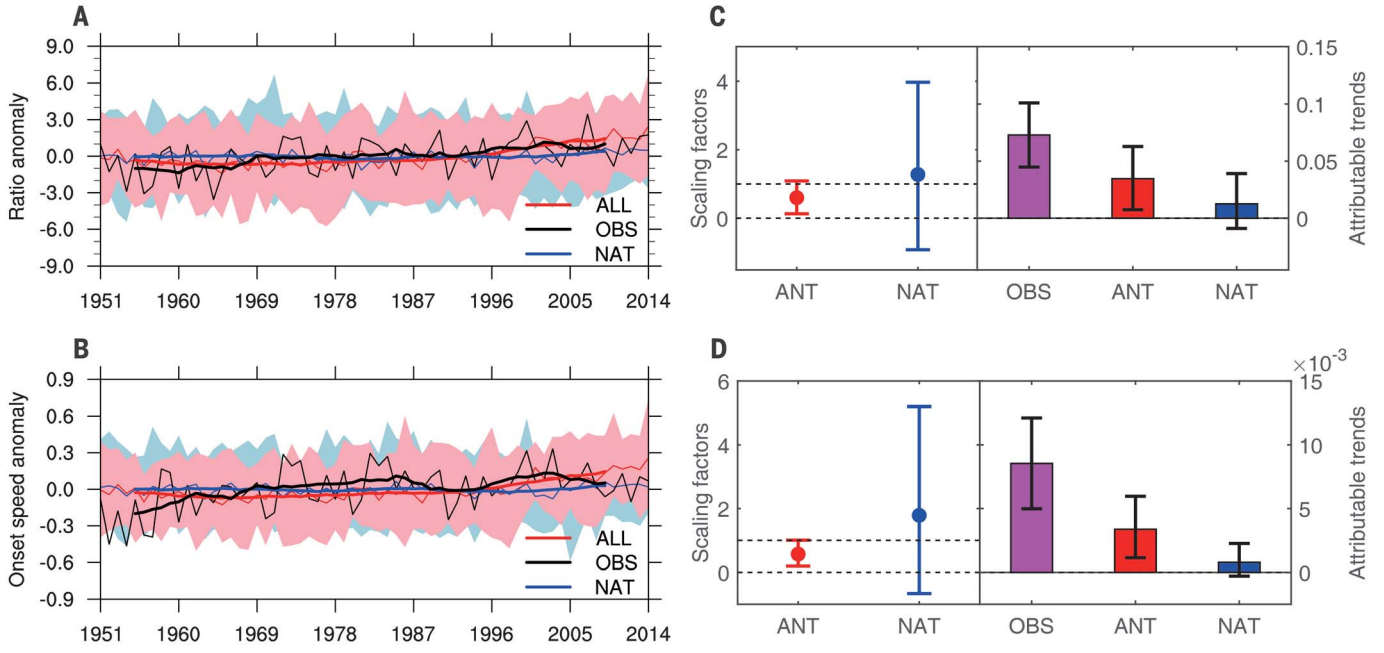

Fig. 2. Attribution for changes in global mean flash drought ratio and onset speed of subseasonal droughts. (**A**) Observed and simulated anomalies of the ratio (%) of flash drought events to subseasonal drought events averaged over the globe from 1951 to 2014. The black line indicates the results based on three global reanalysis datasets (OBS, mean of three reanalyses), and red and blue lines show the ensemble mean results based on CMIP6 climate model simulations with ALL and NAT forcings, respectively (table S1). The thick lines are 10-year running means, and the pink and cyan shadings display the 5 to 95% ranges of ALL and NAT ensemble simulations, respectively. (**C**) The best estimates of the scaling factors (left axis) and attributable increasing trends (%/year, right axis) from two-signal [ANT (ALL-NAT) and NAT] analysis of the changes in flash drought ratio for the period of 1951 to 2014. The time series used for detection and attribution are nonoverlapping 2-year averages (SM, materials and methods). Error bars indicate their corresponding 5 to 95% uncertainty ranges. (**B**) and (**D**) are the same as (A) and (C), except for the anomalies of onset speed of subseasonal droughts (%/pentad), scaling factors, and attributable trends (%/pentad/year) for the changes in onset speed from 1951 to 2014. Ratio and onset speed were identified at each grid cell and then averaged over the globe (excluding Antarctic, Greenland, and deserts) with consideration of the weights of grid areas. All of the statistics were calculated during the growing seasons (April to September for the Northern Hemisphere and October to March for the Southern Hemisphere).

has sped up drought onset and enhanced the global transition to more frequent flash droughts.

Regional drought changes in the past and projected future

A significant global transition to flash droughts is driven by regional increases in flash drought ratio over 74% of the IPCC SREX regions, notably for the significant increases ($P < 0.1$) over East and North Asia, Europe, Sahara, and the west coast of South America (Fig. 3A). Moreover, the onset speed of subseasonal droughts has increased over most regions, with significant increases ($P < 0.1$) over North Asia, Australia, Europe, Sahara, and the west coast of South America (Fig. 3B). These regions' significant increases in flash drought ratio and subseasonal drought onset speed (Fig. 3, A and B) are largely because of the increases in the frequency and onset speed of flash droughts (fig. S12). The regions with increasing onset speed but decreasing flash drought ratio suggest that the transition from slow to flash droughts might not be stable (Fig. 3, A and B). For example, East Africa, Northeast Brazil, and western North America show a historical decline in the flash drought ratio (Fig. 3A), but the frequency increases for both flash and slow droughts (fig. S12, A and C). These regions may eventually switch to a more stable transition once the onset speed increases to a certain level in the future. There are also regions with decreased frequency for both flash and slow droughts (such as eastern North America, southern South America, North Australia, and Southeast Asia), but the drought onset speed has increased (fig. S12). Almost all regions—except the Amazon and West Africa—show increasing trends in flash drought ratio and/or subseasonal drought onset speed (Fig. 3, A and B). For the Amazon, there is no evidence of a transition to flash droughts because drought onset speed decreases and flash-drought frequency decreases, whereas slow-drought frequency increases (fig. S12). For West Africa, both flash and slow droughts increase, whereas flash droughts occur faster and slow droughts occur slower, which suggests a more extreme drought condition even without an obvious transition signal (fig. S12). The results are similar for those with different drought thresholds (figs. S13 to S15).

Because of the regional differences in the responses to global warming, projecting drought changes at the regional scale is more challenging than that at the global scale (*44*–*46*). The CMIP6 climate model ensemble simulations roughly capture the historical changes in flash drought ratio and subseasonal drought onset speed, and 67 and 81% of the IPCC SREX regions show the same trends in ratio and speed between climate models and observations (Fig. 3, A and B, and fig. S16). Under a moderate emission scenario (SSP245) from 2015 to 2100, future projections show significant increasing trends ($P < 0.1$) in the flash drought ratio and subseasonal drought onset speed over almost all IPCC SREX regions (Fig. 3, C and D). Under a higher emission scenario (SSP585), the increasing trends become stronger over most regions (fig. S17). The projection results are similar for different drought thresholds (figs. S18 and S19) and different sets of climate models (fig. S20). Although flash droughts would only increase across 59% of the regions, and slow droughts would decrease over most regions, onset speeds for both flash and slow droughts would increase over most regions (figs. S21 and S22). Therefore, when droughts do occur in the future, they are more likely to be rapid-onset droughts. Although there are

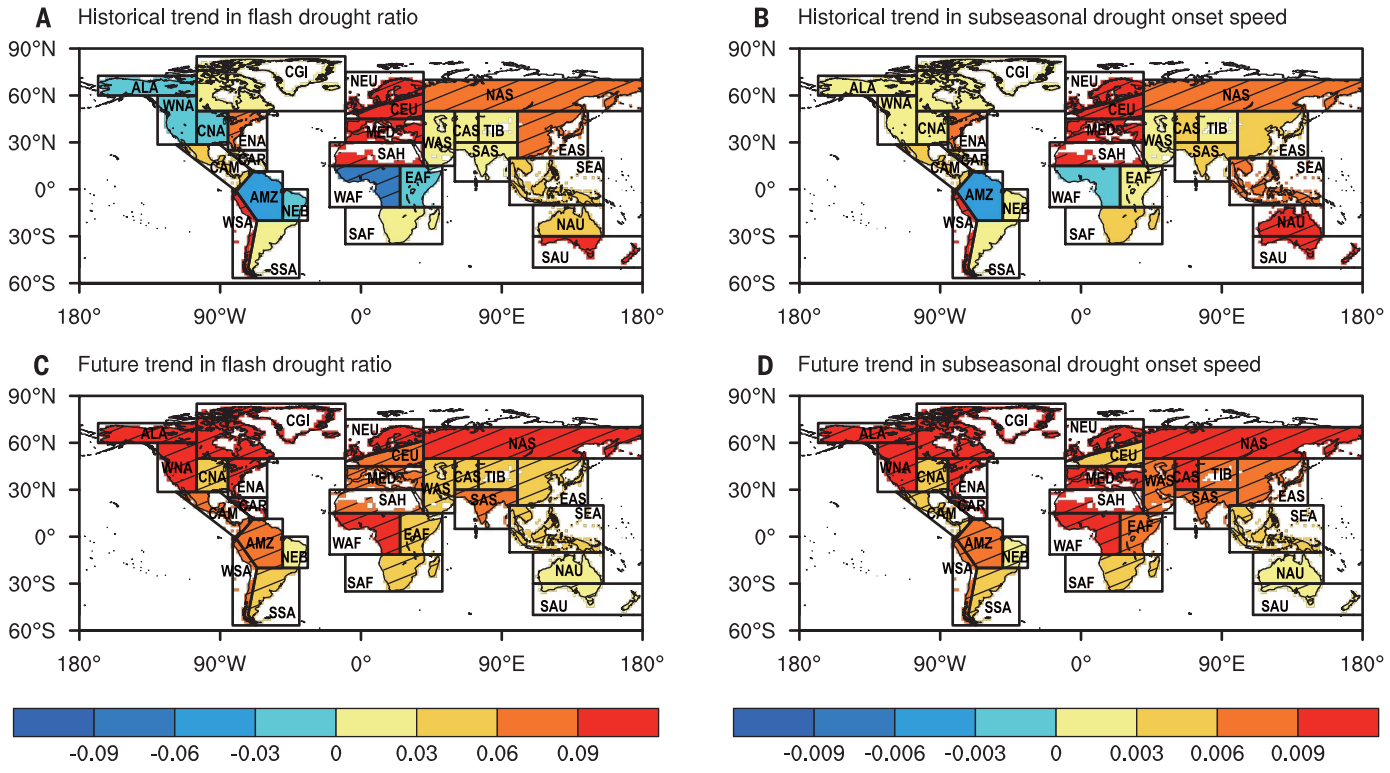

Fig. 3. Historical and future trends in flash drought ratio and onset speed of subseasonal droughts averaged over the IPCC SREX regions. (**A**) Observed trends (%/year) in regional mean ratio of flash drought events to subseasonal drought events from 1951 to 2014 based on the mean time series of three global reanalyses. (**B**) The same as (A), except for the trends (%/pentad/year) in regional mean subseasonal drought onset speed. (**C**) Projected future trends (%/year) in regional mean flash drought ratio from 2015 to 2100 based on CMIP6 climate model ensemble mean simulations under SSP245 scenario. (**D**) The same as (C), except for the trends (%/pentad/year) in regional mean subseasonal drought onset speed. Ratio and onset speed were identified at each grid cell for each model and were then averaged over the IPCC SREX regions with consideration of the weights of grid areas. All of the statistics were calculated during the growing seasons (April to September for the Northern Hemisphere and October to March for the Southern Hemisphere). Hatching represents a significant trend with $P < 0.1$ based on the nonparametric Mann-Kendall test.

uncertainties in the climate model projections, the results suggest that the transition to flash droughts is more stable and rapid in a warmer future, and the higher-emission scenario would lead to a greater risk of flash droughts with quicker onset, which poses a substantial challenge for climate adaptation.

Implications for climate adaptation

The transition toward more frequent flash droughts presents challenges for unraveling the anthropogenic influence on compound extremes (*44*), broadening our understanding of drought impacts (*5*, *37*) across time scales and improving drought prediction capability (*33*) for timely early warning. The increasing drought onset speed primarily comes from intensifying rainfall deficit and increasing evapotranspiration caused by anthropogenic climate change (fig. S10), which dries the soil quickly and creates ideal conditions for heat waves. Because the cooccurrence of heat waves and droughts is increasing globally according to the latest IPCC Sixth Assessment Report (*44*), the anthropogenic-enhanced transition to flash droughts suggests the need to understand flash drought–heat wave interactions both locally and remotely under climate change.

The transition to flash droughts may have irreversible impacts on terrestrial ecosystems (*5*, *37*). The impacts of extreme droughts on vegetation productivity are expected to increase in a warming future (*47*–*49*), but the findings are for long-term droughts with slow evolution. Because flash droughts develop more rapidly with higher temperatures (*27*), ecosystems may not have enough time to adapt to the sudden onset of large water deficits and heat extremes, resulting in a rapid reduction in ecosystem productivity (*37*). In addition, possible future increases in the durations of flash and slow droughts (fig. S23), as well as the increase in total subseasonal drought days caused by the increase in flash drought days (fig. S24), also suggest exacerbated impacts on ecosystems. Assessing such exacerbated impacts will comprehensively broaden our understanding of drought-vegetation interactions at time scales from yearly down to subseasonal.

The acceleration of drought onset also raises substantial challenges for drought monitoring and prediction (*33*). Effective monitoring of subseasonal droughts needs careful and objective selection of drought indices because various types of droughts (such as meteorological, agricultural, and hydrological droughts) also have different implications at the subseasonal time scale. The temporal resolutions of most current monitoring approaches are generally too coarse to capture the onset of flash droughts, and more frequent updates with drought indices suitable for shorter time scales are needed (*33*). For predictions, current approaches are aimed at predicting droughts at seasonal to decadal time scales, depending on oceanic and terrestrial sources of drought predictability (*7*–*10*). For subseasonal drought prediction, the Madden-Julian Oscillation, Southern and Northern Annular Modes, and Indian Ocean Dipole may provide relevant sources of predictability (*33*, *50*), but these large-scale signals should be connected with local synoptic anomalies [through Rossby wave train (*50*)] because most flash droughts do not have a wide spatial coverage. The linkage of these teleconnections with local or remote land-atmospheric coupling (*10*) could

provide a source of predictability for flash droughts.

Anthropogenic climate change is driving the transition to flash droughts, which has a wide range of implications for our understanding of climate change and its impacts, as well as how we can adapt to these changes. Improved understanding is needed for the adaptive capacity of natural ecosystems and human-managed environments that may be more susceptible to flash droughts and associated compound extreme events. Early warning of flash drought onset on time scales of a few weeks can be hugely beneficial for mitigating their impacts and managing the risk of this new normal.

REFERENCES AND NOTES

1. A. K. Mishra, V. P. Singh, *J. Hydrol. (Amst.)* **391**, 202–216 (2010).
2. T. R. Ault, *Science* **368**, 256–260 (2020).
3. A. B. Smith, J. L. Matthews, *Nat. Hazards* **77**, 1829–1851 (2015).
4. X. Yuan, Z. Ma, M. Pan, C. Shi, *Geophys. Res. Lett.* **42**, 4394–4401 (2015).
5. J. A. Otkin *et al*., *Agric. For. Meteorol.* **218-219**, 230–242 (2016).
6. B. I. Cook *et al*., *Wiley Interdiscip. Rev. Clim. Change* **7**, 411–432 (2016).
7. M. Hoerling, A. Kumar, *Science* **299**, 691–694 (2003).
8. G. J. McCabe, M. A. Palecki, J. L. Betancourt, *Proc. Natl. Acad. Sci. U.S.A.* **101**, 4136–4141 (2004).
9. J. K. Roundy, C. R. Ferguson, E. F. Wood, *J. Hydrometeorol.* **14**, 622–635 (2013).
10. R. D. Koster, Y. Chang, H. Wang, S. Schubert, *J. Clim.* **29**, 7345–7364 (2016).
11. A. Dai, *Nat. Clim. Chang.* **3**, 52–58 (2013).
12. A. F. Van Loon *et al*., *Nat. Geosci.* **9**, 89–91 (2016).
13. A. AghaKouchak *et al*, *Rev. Geophys.* **59**, e2019RG000683 (2021).
14. Y. Zhang *et al*., *Remote Sens. Environ.* **222**, 165–182 (2019).
15. X. Zhang *et al*., *Nature* **448**, 461–465 (2007).
16. K. E. Trenberth *et al*., *Nat. Clim. Chang.* **4**, 17–22 (2014).
17. K. Marvel *et al*., *Nature* **569**, 59–65 (2019).
18. Y. Pokhrel *et al*., *Nat. Clim. Chang.* **11**, 226–233 (2021).
19. T. W. Ford, D. B. McRoberts, S. M. Quiring, R. E. Hall, *Geophys. Res. Lett.* **42**, 9790–9798 (2015).
20. X. Yuan, L. Y. Wang, E. F. Wood, *Bull. Am. Meteorol. Soc.* **99**, S86–S90 (2018).
21. X. Yuan *et al*., *Nat. Commun.* **10**, 4661 (2019).
22. S. S. Mahto, V. Mishra, *Environ. Res. Lett.* **15**, 104061 (2020).
23. T. Parker, A. Gallant, M. Hobbins, D. Hoffmann, *Environ. Res. Lett.* **16**, 064033 (2021).
24. Y. Wang, X. Yuan, *Geophys. Res. Lett.* **48**, e2020GL091901 (2021)
25. K. C. Mo, D. P. Lettenmaier, *J. Hydrometeorol.* **17**, 1169–1184 (2016).
26. L. Wang, X. Yuan, Z. Xie, P. Wu, Y. Li, *Sci. Rep.* **6**, 30571 (2016).
27. T. W. Ford, C. F. Labosier, *Agric. For. Meteorol.* **247**, 414–423 (2017).
28. J. A. Otkin *et al*., *Bull. Am. Meteorol. Soc.* **99**, 911–919 (2018).
29. J. I. Christian *et al*., *J. Hydrometeorol.* **20**, 833–846 (2019).
30. M. P. Hoerling *et al*., *Bull. Am. Meteorol. Soc.* **95**, 269–282 (2014).
31. D. J. Lorenz, J. A. Otkin, M. Svoboda, C. R. Hain, Y. Zhong, *J. Geophys. Res. Atmos.* **123**, 8365–8373 (2018).
32. L. G. Chen *et al*., *Atmosphere (Basel)* **10**, 498 (2019).
33. A. G. Pendergrass *et al*., *Nat. Clim. Chang.* **10**, 191–199 (2020).
34. M. Liang, X. Yuan, *Front. Earth Sci. (Lausanne)* **9**, 615969 (2021).
35. NOAA National Centers for Environmental Information (NCEI), "U.S. Billion-Dollar Weather and Climate Disasters 1980-2022" (NCEI, 2022); https://www.ncei.noaa.gov/access/billions/events.pdf.
36. J. A. Otkin *et al*., *Atmosphere (Basel)* **12**, 741 (2021).
37. M. Zhang, X. Yuan, *Hydrol. Earth Syst. Sci.* **24**, 5579–5593 (2020).
38. J. I. Christian *et al*., *Nat. Commun.* **12**, 6330 (2021).
39. V. Eyring *et al*., *Geosci. Model Dev.* **9**, 1937–1958 (2016).
40. S. Seneviratne *et al*., *Managing the Risks of Extreme Events and Disasters to Advance Climate Change Adaptation*, C. B. Field *et al*., Eds. (Cambridge Univ. Press, 2012), pp. 109–230.
41. R. D. Koster, S. D. Schubert, H. Wang, S. P. Mahanama, A. M. DeAngelis, *J. Hydrometeorol.* **20**, 1241–1258 (2019).
42. H. Douville, A. Ribes, B. Decharme, R. Alkama, J. Sheffield, *Nat. Clim. Chang.* **3**, 59–62 (2013).
43. M. Osman *et al*., *Hydrol. Earth Syst. Sci.* **25**, 565–581 (2021).
44. IPCC, Summary for Policymakers in *Climate Change 2021: The Physical Science Basis. Contribution of Working Group I to the Sixth Assessment Report of the Intergovernmental Panel on Climate Change*, V. Masson-Delmotte *et al*., Eds. (Cambridge Univ. Press, 2021).
45. A. M. Ukkola *et al*., *J. Hydrometeorol.* **19**, 969–988 (2018).
46. D. Hoffmann, A. J. E. Gallant, M. Hobbins, *J. Hydrometeorol.* **22**, 1439–1454 (2021).
47. C. Xu *et al*., *Nat. Clim. Chang.* **9**, 948–953 (2019).
48. W. Yuan *et al*., *Sci. Adv.* **5**, eaax1396 (2019).
49. X. Li *et al*., *Nat. Ecol. Evol.* **4**, 1075–1083 (2020).
50. S. D. Schubert, Y. Chang, A. M. DeAngelis, H. Wang, R. D. Koster, *J. Clim.* **34**, 1701–1723 (2021).

ACKNOWLEDGMENTS

Funding: Funding was provided by the National Natural Science Foundation of China 41875105, the National Key R&D Program of China 2018YFA0606002 and 2022YFC3002803, the Natural Science Foundation of Jiangsu Province for Distinguished Young Scholars BK20211540, and the UK-China Research & Innovation Partnership Fund through the Met Office Climate Science for Service Partnership (CSSP) China as part of the Newton Fund. **Author contributions:** Conceptualization: X.Y.; Methodology: X.Y., Y.W., and P.J.; Critical insights: P.W., J.S., and J.A.O.; Writing – original draft: X.Y.; Writing – review and editing: X.Y., Y.W., P.J., P.W., J.S., and J.A.O. **Competing interests:** The authors declare that they have no competing interests. **Data and materials availability:** The soil moisture, precipitation, and evapotranspiration datasets from the GLDAS2.0 land surface reanalysis are available at the GES DISC website for the Catchment land surface model (https://disc.gsfc.nasa.gov/datasets/GLDAS_CLSM10_3H_2.0/summary?keywords=GLDAS) and the Noah land surface model (https://disc.gsfc.nasa.gov/datasets/GLDAS_NOAH10_3H_2.0/summary?keywords=GLDAS). The soil moisture, precipitation and evapotranspiration datasets from ERA5 reanalysis are publicly available at the CDS website for 1951 to 1978 (https://cds.climate.copernicus.eu/cdsapp#!/dataset/reanalysis-era5-single-levels-preliminary-back-extension?tab=form) and for 1979 to 2014 (https://cds.climate.copernicus.eu/cdsapp#!/dataset/reanalysis-era5-single-levels?tab=form). The monthly potential evapotranspiration data produced by GLDAS2.0 are publicly available at https://disc.gsfc.nasa.gov/datasets/GLDAS_NOAH10_M_2.0/summary?keywords=GLDAS. The monthly potential evaporation data produced by ERA-5 are publicly available at the CDS website for 1951 to 1978 (https://cds.climate.copernicus.eu/cdsapp#!/dataset/reanalysis-era5-single-levels-monthly-means-preliminary-back-extension?tab=form) and for 1979 to 2014 (https://cds.climate.copernicus.eu/cdsapp#!/dataset/reanalysis-era5-single-levels-monthly-means?tab=form). The daily soil moisture, precipitation, and evapotranspiration (converted from latent heat flux) data from CMIP5 and CMIP6 are available at the WCRP website (https://esgf-node.llnl.gov/search/cmip5 and https://esgf-node.llnl.gov/projects/cmip6/), and the daily soil moisture data from the CESM1 Large Ensemble are available at the UCAR website (https://www.cesm.ucar.edu/projects/community-projects/LENS/data-sets.html). Statistical methods are noted in the text and figure captions. The computer codes for analyzing data and drawing plots are developed in Fortran or NCAR Command Language (NCL) scripts. The codes for flash and slow droughts are available at https://github.com/Hydroclimate2023/global-flash-drought.

SUPPLEMENTARY MATERIALS

science.org/doi/10.1126/science.abn6301
Materials and Methods
Figs. S1 to S26
Tables S1 to S3
References (*51*–*56*)

Submitted 9 December 2021; accepted 17 February 2023
10.1126/science.abn6301